Ultrahigh-Density Array of Silver Nanoclusters for SERS Substrate with High Sensitivity and Excellent Reproducibility

Won Joon Cho, Youngsuk Kim, and Jin Kon Kim*

National Creative Research Initiative Center for Block Copolymer Self-Assembly, Department of Chemical Engineering, Pohang University of Science and Technology (POSTECH), Pohang, Gyungbuk 790-784, Korea

ABSTRACT

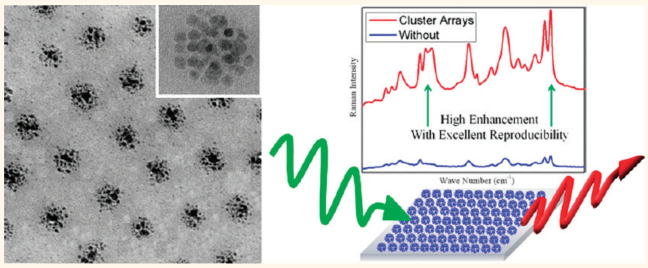

We introduce a simple but robust method to fabricate an ultrahigh-density array of silver nanoclusters for a surface-enhanced Raman spectroscopy (SERS) substrate with high sensitivity and excellent reproducibility at a very large area (wafer scale) based on polystyrene-*block*-poly(4-vinylpyridine) copolymer (PS-*b*-P4VP) micelles. After silver nitrates were incorporated into the micelle cores (P4VP) followed by the reduction to silver nanoclusters, we systematically controlled the gap distance between two neighboring silver nanoclusters ranging from 8 to 61 nm, while the diameter of each silver nanocluster was kept nearly constant (~25 nm). To make a silver nanocluster array with a gap distance of 8 nm, the use of crew-cut-type micelles is required. Fabricated SERS substrate with a gap distance of 8 nm showed very high signal intensity with a SERS enhancement factor as high as 10^8, which is enough to detect a single molecule, and excellent reproducibility (less than ±5%) of the signal intensity. This is because of the uniform size and gap distance of silver nanoclusters in a large area. The substrate could also be used for label-free immunoassays, biosensing, and nanoscale optical antennas and light sources.

KEYWORDS: SERS · silver nanoclusters array · biosensing · high sensitivity and excellent reproducibility · block copolymer micelles

Electromagnetic (EM) fields are intensively localized into a nanoscale junction of noble metals to create tremendous field enhancement, referred to as "hot spots".[1−4] This huge EM field localization resonant coupling with the surface plasmon is essential for surface-enhanced Raman spectroscopy (SERS).[5−12] SERS substrates could be used as label-free immunoassays,[13] biosensing,[14,15] and surface-enhanced spectroscopy.[16] The effect of the gap distance between metallic nanostructures on the SERS has been extensively studied.[17−23] However, great challenges remain in the fabrication of SERS substrates with uniformly narrow gaps of metal nanoparticles in a large area, precise control of the gap distance, and signal reproducibility.

Some research groups generated the hot spots by dropping dilute solutions containing Au (or Ag) nanoparticles on a substrate. However, the locations of the hot spots are very sparse; thus, it is practically impossible to fabricate SERS-active substrates with high sensitivity and good signal reproducibility in a large area.[4,24] Although others have tried to obtain many hot spots or better signal reproducibility by using dimers or trimers of nanoparticles,[25−29] enough signal intensity and excellent signal reproducibility to detect a single molecule have not been achieved so far.

To increase uniformity in the size of the metal nanoparticles and the gap distance between two neighboring nanostructures, focused-ion-beam[30,31] and electron-beam lithography[32,33] have been usually used to prepare the SERS substrates. But in this case, it is not easy to decrease the gap distance down to sub-10 nm, which is known for obtaining high signal intensity for a SERS substrate.[31−35] In addition, since the fabrication of metal nanostructure arrays in a large area is time-consuming and expensive, the area containing metal nanostructures is very limited (smaller than 100 μm^2).

Some research groups[36,37] have fabricated SERS substrates in a large area having reproducible SERS intensity. Que *et al.*[36] prepared a gold nanoparticle assembly on a

* Address corresponding to jkkim@postech.ac.kr.

Received for review September 12, 2011 and accepted November 26, 2011.

Published online November 26, 2011
10.1021/nn2035236

silicon wafer by using capillary force. However, the actual area covered with gold nanoparticles in the wafer was very small (3600 μm^2). In addition, neighboring gold nanoparticles could be aggregated because the surfactants were completely removed at a high temperature (400 °C). Qian *et al.*[37] fabricated a petal-like arrayed structure by using a self-assembled bilayer of silica nanoparticles and anisotropic physical vapor deposition, and the substrate showed a high SERS enhancement factor (EF). While the detection by a laser for SERS intensity was limited within a circle with a diameter of 1 μm, the smallest diameter of silica nanoparticles was 250 nm. Thus, the deviation of the number of hot spots could be as large as 25%, which means that a high reproducibility of the SERS intensity is not easy to obtain for this array.

Other research groups reported the fabrication of a SERS substrate based on block copolymer self-assembly.[38−40] Wang *et al.*[38] fabricated a mushroom-like gold structure by galvanic displacement reaction on a nanoporous template based on polystyrene-*block*-poly(2-vinylpyridine) copolymer (PS-*b*-P2VP). Liz-Marzán and co-workers[39] fabricated a SERS substrate with a silver nanoparticle array. For this purpose, gold nanodots were first prepared by the coordination of $HAuCl_4$ with pyridine groups in P2VP micelle cores followed by the reduction. Then the silver nanoparticles were grown on the pre-existing gold nanodots by chemical reaction to control the gap distance between neighboring silver nanoparticles. Lee *et al.*[40] fabricated a SERS substrate with a gold nanoparticle array in a large area by utilizing perpendicularly oriented cylindrical microdomains of poly(4-vinylpyridine) (P4VP) in polystyrene-*block*-P4VP copolymer (PS-*b*-P4VP) thin film. Then, P4VP blocks were positively quaternized to accommodate presynthesized gold nanoparticles with negatively charged citrate functional groups. Gold was further overgrown on the pre-existing gold nanoparticles in P4VP microdomains by immersing the substrate in the solution containing a gold precursor of $HAuCl_4$.

Although the array of the silver or gold nanostructures was prepared in a large area by using block copolymer self-assembly, all of the investigations reported in the literature[38−40] should use an additional metal growing step, for instance, dipping of the substrate into solutions containing metal precursors, on the pre-existing seeds of gold nanodots (or nanoparticles). However, during this step, the pre-existing gold nanoparticle seeds might be dissolved in addition to the possible formation of nanoparticles at nonseeding positions. Thus, excellent structure uniformity in the gap distance and the size (or shape) of nanoparticles in the array in a large area, which is the most important merit of the use of block copolymer self-assembly, could not be obtained. Due to the nonuniformity in nanoparticle structures, the reported EF value is at most $\sim 10^6$. Also, the reproducibility in the SERS signal was not good.

Thus, the easy and cheap fabrication of SERS substrates in a large area, while maintaining high EF to detect single molecules[41,42] and excellent reproducibility of signal intensity (less than $\pm$5%), still remains challenging. Also, to investigate directly the effect of the gap distance of neighboring metal nanoparticles on Raman intensity enhancement, the hot spot density should be very large and uniform through the entire SERS substrate. The easiest and most robust method to achieve these requirements is to prepare an ultrahigh-density array of silver nanoclusters (or nanoparticles) having sub-10 nm gap distance between two neighboring nanoparticles in a very large area (at least cm^2). We realize that when the crew-cut-type block copolymer micelles[43] with shorter corona size compared with the core size are used, the nanoparticle array with a sub-10 nm gap distance is easily fabricated. In this situation, we could maintain excellent features of the block copolymer self-assembly to obtain a uniform gap distance and size of nanoparticles in a large area, because an addition metal growing step is not needed.

In this study, we chose PS-*b*-P4VP micelles since the precursor of silver nitrate ($AgNO_3$) was easily incorporated by the coordination with pyridine groups in the P4VP micelle cores. Although many different metal and semiconducting materials were easily incorporated into spherical micelles of P4VP in PS-*b*-P4VP,[44−48] the direct inclusion of silver precursors followed by the reduction to silver nanoparticles (or nanoclusters) and an array with a smaller gap distance (say, less than 10 nm), which is required to achieve the hot spots, have not been reported in the literature. This is because only normal PS-*b*-P4VP or PS-*b*-P2VP micelles, which have a longer corona size compared to the core size, have been used to prepare silver or gold nanoparticles in the previous reports.[44−48]

We also used various PS-P4VPs with different block ratios of PS and P4VP chains to control the gap distance (*d*) between two neighboring silver nanoclusters from 8 to 61 nm, while the average diameter (*D*) of all of the silver nanoclusters was kept nearly constant ($\sim$25 nm). The substrate with an ultrahigh-density array of silver nanoclusters showed very high SERS intensity with an EF as high as 1×10^8 and excellent reproducibility in the signal (less than $\pm$5%). Since a single molecule could be detected with a substrate having an excellent EF,[41,42] the SERS substrate fabricated in this study could be very effective in detecting a single molecule needed for label-free immunoassays and biosensors. Also, this substrate could be used for nanoscale optical antenna,[49,50] light sources,[51] and lithographic tools.[52]

RESULTS AND DISCUSSION

Figure 1 gives a schematic of the preparation of an ultrahigh-density array of silver nanoclusters on a silicon

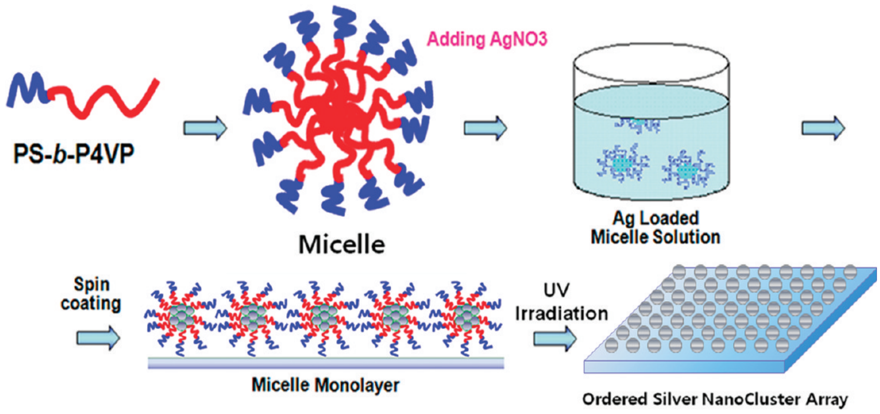

Figure 1. Scheme of the fabrication of an ultrahigh-density array of silver nanoclusters on a silicon wafer.

TABLE 1. Values of *D* and *d* Prepared by Different PS-*b*-P4VPs after UV Treatment without and with Oxygen Plasma Treatment for 2 min

sample code	used PS-*b*-P4VPs (molecular weights of PS and P4VP block)	diameter of silver nanocluster (*D*) and gap distance (*d*)	without plasma treatment	oxygen plasma treatment for 2 min
C1	10 400-*b*-19 200	*D*	24.5 ± 1.7 nm	20.6 ± 1.8 nm
		d	8.3 ± 1.4 nm	10.4 ± 2.4 nm
C2	19 000-*b*-22 000	*D*	24.4 ± 1.8 nm	20.9 ± 1.9 nm
		d	20.4 ± 1.0 nm	24.1 ± 2.1 nm
C3	35 000-*b*-21 000	*D*	24.9 ± 1.5 nm	20.9 ± 2.1 nm
		d	34.6 ± 1.2 nm	38.1 ± 2.4 nm
C4	41 500-*b*-17 500	*D*	24.6 ± 1.8 nm	20.3 ± 2.2 nm
		d	44.6 ± 1.1 nm	47.9 ± 2.1 nm
C5	122 000-*b*-22 000	*D*	24.8 ± 2.1 nm	20.3 ± 1.7 nm
		d	61.2 ± 1.5 nm	64.8 ± 2.5 nm

wafer by using PS-*b*-P4VP micelles. First, PS-*b*-P4VP was dissolved into toluene/tetrahydrofuran (THF) mixed solvent. THF is necessary for the crew-cut micelles with short chain length of the corona (PS block chains), whereas only toluene was used for normal micelles with longer PS block lengths (the details are in section 1 in the Supporting Information). Once the spherical micelles with P4VP cores were formed, $AgNO_3$ was incorporated into the micelle core and reduced to silver nanoclusters (or nanoparticles) by using $NaBH_4$.[53] Next, the micelle solutions with silver nanoclusters were spin-coated on a silicon wafer, followed by the complete removal of the block copolymer thin film by UV irradiation at room temperature. To change the gap (or interparticle) distance between two neighboring silver nanoclusters, we employed five different PS-*b*-P4VPs with various block ratios of PS and P4VP blocks (see Table 1). Since the molecular weight of the P4VP block in all block copolymers was almost the same, the core diameter of the silver nanoclusters (nanoparticles) was kept nearly constant.

Figure 2 gives the field emission scanning electron microscopy (FE-SEM) images of the arrays of silver nanoclusters obtained from four different PS-*b*-P4VPs, after the complete removal of PS-*b*-P4VPs. We found that the silver nanoclusters are hexagonally packed, and the size of the nanocluster is very uniform over the entire substrate (wafer scale). Also, *D* was almost the same regardless of different PS-*b*-P4VPs, whereas *d* increased gradually with increasing the molecular weight of the PS corona block. The values of the *D* and *d* are determined by FE-SEM images by counting at least 250 silver nanoclusters (see Figure S2 in the Supporting Information) and given in Table 1.

One interesting feature in the insets of Figure 2 is that each silver nanocluster contains several tiny silver nanoparticles (see also Figure S3 in the Supporting Information for enlarged images). To study the effect of the particle shape on SERS intensity, the sample was further treated by oxygen plasma at room temperature for certain time intervals. As shown in Figure 3, the silver nanocluster becomes a single silver nanoparticle when the sample was treated by oxygen plasma at room temperature for 2 min. The values of *D* and *d* for the samples treated by oxygen plasma for 1 min are given in Table S2 of the Supporting Information.

Figure 4 shows SERS spectra of crystal violet (CV) adsorbed on the silver nanocluster arrays, measured with a Raman microscope at 514.5 nm excitation and a laser spot of ~1.54 μm^2. CV is a well-known molecule for SERS study because it efficiently chemisorbs on the silver surfaces by the existence of an amino group.[54,55] The SERS spectra reveal the characteristic peaks of

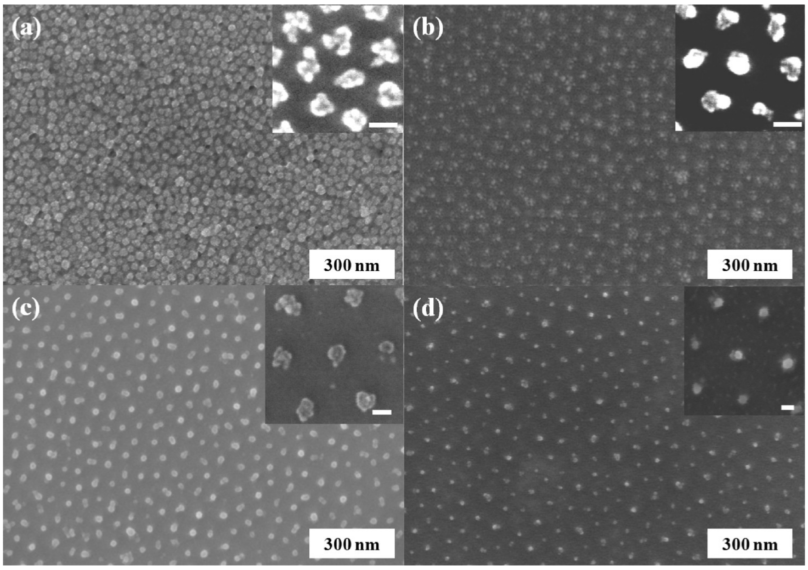

Figure 2. FE-SEM images of silver nanocluster arrays prepared by four different PS-*b*-P4VPs: (a) C1, (b) C2, (c) C4, and (d) C5. The scale bar in each inset is 30 nm. The number-average molecular weights of PS and P4VP blocks for C1−C5 are given in Table 1.

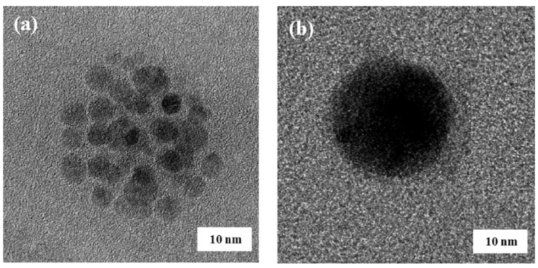

Figure 3. HR-TEM images of one silver nanocluster in sample C1 without (a) and with oxygen plasma treatment at room temperature for 2 min (b).

CV at 1172, 1371, and 1619 cm^{-1}. The SERS signals increased dramatically with decreasing *d*, because the electromagnetic coupling between the naoclusters dramatically increases with decreasing gap distance.[12] We also employed two nonresonant SERS molecules, 1,2-di-(4-pyridyl)ethylene (BPE) and 4-aminothiolphenol (4-ATP). Both molecules do not give any resonance at 514.5 nm. We find that the effects of the gap distance and oxygen plasma treatment on the SERS intensity and EF values for these two nonresonant SERS molecules are similar to those of CV, although the SERS intensity and the EF were slightly decreased (20−30%) compared with those of CV (see Figures S7−S10 in the Supporting Information). Thus, we consider that the SERS substrates employed in this study have excellent SERS properties of both resonant and nonresonant SERS molecules.

The increased SERS intensity with decreasing *d* is also consistent with the red-shift of the peak position at ~500 nm in the UV−visible absorption spectra (see Figures S11 and S12 in the Supporting Information). The peak in the UV−visible spectra corresponds to the coupling wavelength at which the surface plasmon resonance (SPR) is maximized. Since the excitation

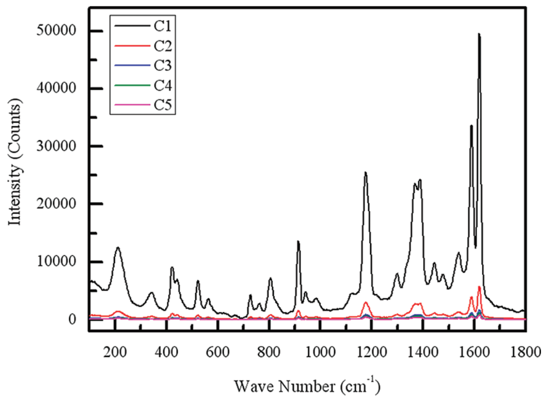

Figure 4. SERS spectra of CV for the silver nanocluster arrays prepared by five different PS-*b*-P4VPs.

wavelength used in the SERS measurement was 514.5 nm, the red-shift in the UV−visible spectra indicates the better coupling between the incident light and surface plasmon, resulting in a higher SERS intensity.[56−58]

Quantification of the EF in a SERS substrate is not trivial and needs some assumptions since the number of adsorbed molecules is poorly defined.[56,57] In this study, we assume that CV molecules are uniformly adsorbed on the silver nanoclusters (see section 2 in the Supporting Information). Figure 5 shows the calculated EF for silver nanocluster (and nanoparticle) arrays depending on *d*. The details for the EF calculation are also given in section S2 of the Supporting Information. With decreasing *d*, the electromagnetic coupling between the nanoclusters increases the Raman spectra.[12] For the substrates with a silver nanocluster array, EF was lower (~3.3 × 10^5) at *d* larger than 35 nm. At $d \approx 20$ nm, EF increased significantly, to ~10^7. The largest

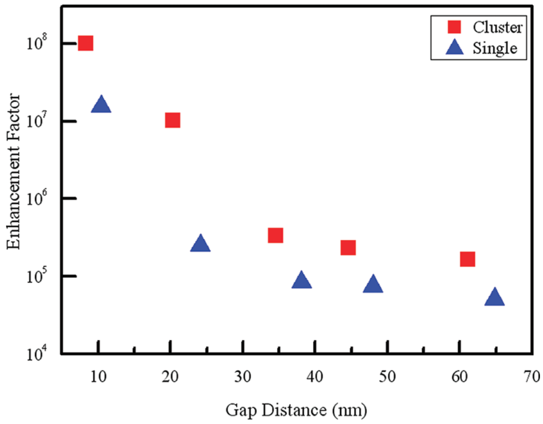

Figure 5. SERS enhancement factor of CV for the silver nanocluster and single silver nanoparticle arrays at various gap distnaces (*d*).

SERS EF was $\sim10^8$ at a $d \approx 8$ nm. On the other hand, for other substrates with an ultrahigh-density array of silver nanoparticle, EF at $d \approx 24$ nm was still low ($\sim2.5 \times 10^5$). A large EF ($\sim1.5 \times 10^7$) was observed only at a d of ~10 nm.

Thus, the critical gap distance below which EF increases significantly depends on the shape of the silver (nanocluster with tiny nanoparticles *versus* single nanoparticle). For the SERS substrates with silver nanoparticles, the critical gap distance would be ~10 nm. However, very interestingly, for the SERS substrates with an ultrahigh-density array of silver nanoclusters, a significant increase in EF was observed even at $d \approx 20$ nm, athough the EF at $d \approx 8$ nm is ~10 times larger than that at $d \approx 20$ nm. This indicated that the Raman intensity was affected by not only d but also the internal silver nanocluster structure.[58−62] Even though the diameter of tiny silver nanoparticles inside a single nanocluster was ~4 nm, these tiny nanoparticles could interact with each other, which results in a contribution to the SERS intensity. Namely, the array of silver nanoclusters increased plasmon coupling among individual tiny nanoparticles in the nanocluster, which is similar to the multiscale SERS signal enhancement.[58,62]

Since the Raman intensity reflects from all of the nanoclusters within the laser spot, the measured intensity was quite reproducible (less than $\pm5\%$ over 30 experiments). The values of standard deviation in EF for all the substrates are given in Table S3 of the Supporting Information. Excellent reproducibility is attributed to the fact that a large number of silver nanoclusters (and, thus, hot spots) ranging from 250 to 1500 contributed Raman spectra within the laser spot ($\sim1.54\ \mu m^2$) as well as very good uniformity in the gap distance and silver nanocluster size.

In conclusion, we fabricated a SERS substrate with high sensitivity and excellent reproducibility by using an ultrahigh-density array of silver nanoclusters based on block copolymer micelles. For the SERS substrates with silver nanoparticles, the critical gap distance was ~10 nm and the EF was $\sim1.5 \times 10^7$. However, for the SERS substrates with an ultrahigh density array of silver nanoclusters, a significant increase in EF was observed even at a gap distance of ~20 nm. At a gap distance of ~8 nm, the EF was as high as 1.0×10^8, which is large enough to detect a single molecule. Furthermore, excellent reproducibility (less than $\pm5\%$) was achieved over a large area (wafer scale). This is because a large number of silver nanoclusters (and, thus, hot spots) ranging from 250 to 1500 contributed Raman spectra within the laser spot as well as excellent uniformity in gap distance and silver nanocluster size resulting from the excellent feature of the block copolymer self-assembly. Due to easy and robust fabrication in a large area, the substrate fabricated in this study could be used for label-free immunoassays, biosensing, and nanoscale optical antennas and light sources.

EXPERIMENTAL SECTION

Fabrication of an Ultrahigh-Density Array of Silver Nanoclusters. We used five different PS-*b*-P4VPs (Polymer Source Inc.) with different PS and P4VP blocks to change the gap (or interparticle) distance of silver nanoparticles. The number-average molecular weight (M_n) of the P4VP block in all block copolymers was nearly constant to obtain a similar core diameter. The gap distance of two neighboring silver nanoclusters was carefully controlled by using different molecular weight PS blocks. For the crew-cut type micelles where the corona block (PS) is shorter than the core block (P4VP), it is not easy to have well-defined micelles when only toluene is used. Thus, in this situation, we added THF, which is a selective solvent of PS block, to the toluene solution, to facilitate the easy and stable formation of the P4VP micelles. The amount of THF in the mixed solvent was increased with decreasing molecular weight of the PS block in PS-*b*-P4VPs (see Table S1 in the Supporting Information).

After each block copolymer was added to the mixed solvent (0.5 wt % in solid), it was stirred for 3 h at room temperature. Then the solution temperature was increased to 70 °C and held at this temperature for 2 h. The use of high temperature is required for stable formation of the crew-cut micelles.

To incorporate the silver precursor into the P4VP micelle core, an excess amount of $AgNO_3$ (molar ratio of $AgNO_3$ to vinyl pyridine monomer = 2) was added to the micelle solution and stirred for 24 h at room temperature to facilitate the coordination between silver ions (Ag^+) and poly(4-vinylpyridine) chains. Then, $NaBH_4$ (Sigma-Aldrich) was added and stirred for a further 24 h to reduce the coordinated silver ions to silver nanoparticles (or nanoclusters). The noncoordinated silver ions were precipitated as big particles after the reduction by $NaBH_4$. These big silver particles were completely removed by using a PTFE syringe filter (size of 400 nm). Finally, the micelle solutions were spin-coated at a rotating speed of 2000 rpm for 60 s on a silicon wafer, which produced the monolayer of the P4VP spherical micelles.

Characterization. The morphologies of the micelles were investigated by transmission electron microscopy (TEM, Hitachi Ltd., S-7600), operating at 3 kV, after the sample was stained with iodine (I_2) for 1 h. The gap distance and diameters of the silver nanoclusters after the removal of block copolymer thin films were determined by scanning electron microscopy (SEM, Hitachi, S4800) operating at 10 kV. High-resolution transmission electron microscopy (HR-TEM, JEOL, JEM-2100F) operating at 300 kV was also employed to observe the inner structure of a single nanocluster. PS-*b*-P4VP was removed by UV irradiation using a UV lamp (model G15T8, Sankyo Denki, Japan) with the highest intensity at 253.7 nm for 24 h under air at room temperature. We confirmed via Fourier transform infrared spectroscopy (FT-IR) (Nicolet 700) that the block copolymer film was completely removed after UV irradiation for 24 h (see Figure S13 in the Supporting Information).

To control the shape of the silver nanoclusters, the sample was further treated by oxygen plasmas at room temperature. The specimen was placed in a vacuum chamber (Plasma Prep II, Spi) maintaining an O_2 pressure of 100 mTorr and 50 mW rf power. The silvers in the nanoclusters were not oxidized after oxygen plasma treatment for 2 min, which was confirmed by energy dispersive X-ray spectroscopy (EDX: JEOL JEM-2100F) (see Figure S14 in the Supporting Information).

Raman intensity was measured in a backscattering geometry by using a JY LabRam HR fitted with a liquid-nitrogen-cooled CCD detector. The spectra were collected under ambient conditions using the 514.5 nm line of an Ar-ion laser with 0.05 mW irradiation of the sample surface. The acquisition time was 20 s. The radius of the laser spot was 0.70 μm; thus, the laser spot area was 1.54 μm^2. The SERS molecules employed in this study, CV, BPE, and 4-ATP, were purchased from Aldrich Chemical Co.

Acknowledgment. This work was supported by the National Creative Research Initiative Program of the National Research Foundation of Korea.

Supporting Information Available: Experimental details and the estimation of EF, FE-SEM and HR-TEM images, SERS intensity, UV−vis, FT-IR and EDX spectra. This material is available free of charge *via* the Internet at http://pubs.acs.org.

REFERENCES AND NOTES

1. Moskovits, M. Surface-Enhanced Raman Spectroscopy: A Brief Retrospective. *J. Raman Spectrosc.* **2005**, *36*, 485–496.
2. Bosnick, K. A.; Jiang., J.; Brus., L. E. Fluctuations and Local Symmetry in Single-Molecule Rhodamine 6G Raman Scattering on Silver Nanocrystal Aggregates. *J. Phys. Chem. B* **2002**, *106*, 8096–8099.
3. Otto, A. What Is Observed in Single Molecule SERS, and Why? *J. Raman Spectrosc.* **2002**, *33*, 593–598.
4. Camden, J. P.; Dieringer, J. A.; Wang, Y.; Masiello, D. J.; Marks, L. D.; Schatz, G. C.; Van Duyne, R. P. Probing the Structure of Single-Molecule Surface-Enhanced Raman Scattering Hot Spots. *J. Am. Chem. Soc.* **2008**, *130*, 12616–12617.
5. Moskovits, M. Surface-Enhanced Spectroscopy. *Rev. Mod. Phys.* **1985**, *57*, 783–826.
6. Michaels, A. M.; Jiang; Brus, L. Ag Nanocrystal Junctions as the Site for Surface-Enhanced Raman Scattering of Single Rhodamine 6G Molecules. *J. Phys. Chem. B* **2000**, *104*, 11965–11971.
7. Xu, H.; Aizpurua, J.; Käll, M.; Apell, P. Electromagnetic Contributions to Single-Molecule Sensitivity in Surface-Enhanced Raman Scattering. *Phys. Rev. E* **2000**, *62*, 4318–4324.
8. Tian, Z.-Q.; Ren, B.; Wu, D.-Y. Surface-Enhanced Raman Scattering: From Noble to Transition Metals and from Rough Surfaces to Ordered Nanostructures. *J. Phys. Chem. B* **2002**, *106*, 9463–9483.
9. Tao, A.; Kim, F.; Hess, C.; Goldberger, J.; He, R.; Sun, Y.; Xia, Y.; Yang, P. Langmuir−Blodgett Silver Nanowire Monolayers for Molecular Sensing Using Surface-Enhanced Raman Spectroscopy. *Nano Lett.* **2003**, *3*, 1229–1233.
10. Willets, K. A.; Van Duyne, R. P. Localized Surface Plasmon Resonance Spectroscopy and Sensing. *Annu. Rev. Phys. Chem.* **2007**, *58*, 267–297.
11. Le, F.; Brandl, D. W.; Urzhumov, Y. A.; Wang, H.; Kundu, J.; Halas, N. J.; Aizpurua, J.; Nordlander, P. Metallic Nanoparticle Arrays: A Common Substrate for Both Surface-Enhanced Raman Scattering and Surface-Enhanced Infrared Absorption. *ACS Nano* **2008**, *2*, 707–718.
12. García-Vidal, F. J.; Pendry, J. B. Theory for Surface Enhanced Raman Scattering. *Phys. Rev. Lett.* **1996**, *77*, 1163.
13. Schultz, S.; Smith, D. R.; Mock, J. J.; Schultz, D. A. Single-Target Molecule Detection with Nonbleaching Multicolor Optical Immunolabels. *Proc. Natl. Acad. Sci. U. S. A.* **2000**, *97*, 996–1001.
14. Anker, J. N.; Hall, W. P.; Lyandres, O.; Shah, N. C.; Zhao, J.; Van Duyne, R. P. Biosensing with Plasmonic Nanosensors. *Nat. Mater.* **2008**, *7*, 442–453.
15. Wang, Y.; Seebald, J. L.; Szeto, D. P.; Irudayaraj, J. Biocompatibility and Biodistribution of Surface-Enhanced Raman Scattering Nanoprobes in Zebrafish Embryos: In Vivo and Multiplex Imaging. *ACS Nano* **2010**, *4*, 4039–4053.
16. Chen, Y.; Munechika, K.; Ginger, D. S. Dependence of Fluorescence Intensity on the Spectral Overlap between Fluorophores and Plasmon Resonant Single Silver Nanoparticles. *Nano Lett.* **2007**, *7*, 690–696.
17. Fleischmann, M.; Hendra, P. J.; McQuillan, A. J. Raman Spectra of Pyridine Adsorbed at a Silver Electrode. *Chem. Phys. Lett.* **1974**, *26*, 163–166.
18. Jeanmaire, D. L.; Van Duyne, R. P. Surface Raman Spectroelectrochemistry: Part I. Heterocyclic, Aromatic, and Aliphatic Amines Adsorbed on the Anodized Silver Electrode. *J. Electroanal. Chem.* **1977**, *84*, 1–20.
19. Haynes, C. L.; McFarland, A. D.; Duyne, R. P. V Surface-Enhanced Raman Spectroscopy. *Anal. Chem.* **2005**, *77*, 338–346.
20. Li, S.; Pedano, M. L.; Chang, S.-H.; Mirkin, C. A.; Schatz, G. C. Gap Structure Effects on Surface-Enhanced Raman Scattering Intensities for Gold Gapped Rods. *Nano Lett.* **2010**, *10*, 1722–1727.
21. Li, J. F.; Huang, Y. F.; Ding, Y.; Yang, Z. L.; Li, S. B.; Zhou, X. S.; Fan, F. R.; Zhang, W.; Zhou, Z. Y.; WuDe, Y.; *et al*. Shell-Isolated Nanoparticle-Enhanced Raman Spectroscopy. *Nature* **2010**, *464*, 392–395.
22. Fan, M.; Andrade, G. F. S.; Brolo, A. G. A Review on the Fabrication of Substrates for Surface Enhanced Raman Spectroscopy and Their Applications in Analytical Chemistry. *Anal. Chim. Acta* **2011**, *693*, 7–25.
23. Halas, N. J.; Lal, S.; Chang, W.-S.; Link, S.; Nordlander, P. Plasmons in Strongly Coupled Metallic Nanostructures. *Chem. Rev.* **2011**, *111*, 3913–3961.
24. Farah, A. A.; Bravo-Vasquez, J. P.; Alvarez-Puebla, R. A.; Cho, J. Y.; Fenniri, H. Robust Au-PEG/PS Microbeads as Optically Stable Platforms for SERS. *Small* **2009**, *5*, 1283–1286.
25. Talley, C. E.; Jackson, J. B.; Oubre, C.; Grady, N. K.; Hollars, C. W.; Lane, S. M.; Huser, T. R.; Nordlander, P.; Halas, N. J. Surface-Enhanced Raman Scattering from Individual Au Nanoparticles and Nanoparticle Dimer Substrates. *Nano Lett.* **2005**, *5*, 1569–1574.
26. Li, W.; Camargo, P. H. C.; Lu, X.; Xia, Y. Dimers of Silver Nanospheres: Facile Synthesis and Their Use as Hot Spots for Surface-Enhanced Raman Scattering. *Nano Lett.* **2008**, *9*, 485–490.
27. Chen, G.; Wang, Y.; Yang, M.; Xu, J.; Goh, S. J.; Pan, M.; Chen, H. Measuring Ensemble-Averaged Surface-Enhanced Raman Scattering in the Hotspots of Colloidal Nanoparticle Dimers and Trimers. *J. Am. Chem. Soc.* **2010**, *132*, 3644–3645.
28. Jin, R. Nanoparticle Clusters Light Up in SERS. *Angew. Chem., Int. Ed.* **2010**, *49*, 2826–2829.
29. Lee, S. Y.; Hung, L.; Lang, G. S.; Cornett, J. E.; Mayergoyz, I. D.; Rabin, O. Dispersion in the SERS Enhancement with Silver Nanocube Dimers. *ACS Nano* **2010**, *4*, 5763–5772.
30. Ebbesen, T. W.; Lezec, H. J.; Ghaemi, H. F.; Thio, T.; Wolff, P. A. Extraordinary Optical Transmission through Sub-Wavelength Hole Arrays. *Nature* **1998**, *391*, 667–669.
31. Tseng, A. A. Recent Developments in Nanofabrication Using Focused Ion Beams. *Small* **2005**, *1*, 924–939.
32. Altewischer, E.; van Exter, M. P.; Woerdman, J. P. Plasmon-Assisted Transmission of Entangled Photons. *Nature* **2002**, *418*, 304–306.
33. Abu Hatab, N. A.; Oran, J. M.; Sepaniak, M. J. Surface-Enhanced Raman Spectroscopy Substrates Created via Electron Beam Lithography and Nanotransfer Printing. *ACS Nano* **2008**, *2*, 377–385.
34. Gopinath, A.; Boriskina, S. V.; Premasiri, W. R.; Ziegler, L.; Reinhard, B. M.; Dal Negro, L. Plasmonic Nanogalaxies:

Multiscale Aperiodic Arrays for Surface-Enhanced Raman Sensing. *Nano Lett.* **2009**, *9*, 3922–3929.
35. Im, H.; Bantz, K. C.; Lindquist, N. C.; Haynes, C. L.; Oh, S. H. Vertically Oriented Sub-10-nm Plasmonic Nanogap Arrays. *Nano Lett.* **2010**, *10*, 2231–2236.
36. Que, R.; Shao, M.; Zhuo, S.; Wen, C.; Wang, S.; Lee, S.-T. Highly Reproducible Surface-Enhanced Raman Scattering on a Capillarity-Assisted Gold Nanoparticle Assembly. *Adv. Funct. Mater.* **2011**, *21*, 3337–3343.
37. Qian, C.; Ni, C.; Yu, W.; Wu, W.; Mao, H.; Wang, Y.; Xu, J. SERS: Highly-Ordered, 3D Petal-Like Array for Surface-Enhanced Raman Scattering. *Small* **2011**, *7*, 1801–1806.
38. Wang, Y.; Becker, M.; Wang, L.; Liu, J.; Scholz, R.; Peng, J.; Gösele, U.; Christiansen, S.; Kim, D. H.; Steinhart, M. Nanostructured Gold Films for SERS by Block Copolymer-Templated Galvanic Displacement Reactions. *Nano Lett.* **2009**, *9*, 2384–2389.
39. Sánchez-Iglesias, A.; Aldeanueva-Potel, P.; Ni, W.; Pérez-Juste, J.; Pastoriza-Santos, I.; Alvarez-Puebla, R. A.; Mbenkum, B. N.; Liz-Marzán, L. M. Chemical Seeded Growth of Ag Nanoparticle Arrays and Their Application as Reproducible SERS Substrates. *Nano Today* **2010**, *5*, 21–27.
40. Lee, W.; Lee, S. Y.; Briber, R. M.; Rabin, O. Self-Assembled SERS Substrates with Tunable Surface Plasmon Resonances. *Adv. Funct. Mater.* **2011**, *21*, 3424–3429.
41. Etchegoin, P. G.; Le Ru, E. C. A Perspective on Single Molecule SERS: Current Status and Future Challenges. *Phys. Chem. Chem. Phys.* **2008**, *10*, 6079–6089.
42. Pieczonka, N. P. W; Aroca, R. F. Single Molecule Analysis by Surfaced-Enhanced Raman Scattering. *Chem. Soc. Rev.* **2008**, *37*, 946–954.
43. Zhang, L.; Eisenberg, A. Multiple Morphologies of "Crew-Cut" Aggregates of Polystyrene-b-Poly(acrylic acid) Block Copolymers. *Science* **1995**, *268*, 1728–1731.
44. Förster, S.; Antonietti, M. Amphiphilic Block Copolymers in Structure-Controlled Nanomaterial Hybrids. *Adv. Mater.* **1998**, *10*, 195–217.
45. Anthony, S. P.; Kim, J. K. Two-Dimensional Arrays of Luminescent Metal-Selenide Nanoparticle. *Chem. Commun.* **2008**, *14*, 1193–1195.
46. Anthony, S. P.; Cho, W. J.; Lee, J. I.; Kim, J. K. Synthesis of Lead Chalcogenide Nanoparticles in Block Copolymer Micelles: Investigation of Optical Properties and Fabrication of 2-D Arrays of Nanoparticles. *J. Mater. Chem.* **2009**, *19*, 280–285.
47. Kim, J. K.; Lee, J. I.; Lee, D. H. Self-Assembled Block Copolymers: Bulk to Thin Film. *Macromol. Res.* **2008**, *16*, 267–292.
48. Kim, J. K.; Yang, S. Y.; Lee, Y. M.; Kim, Y. S. Functional Nanomaterials Based on Block Copolymer Self-Assembly. *Prog. Polym. Sci.* **2010**, *35*, 1325–1349.
49. Sundaramurthy, A.; Schuck, P. J.; Conley, N. R.; Fromm, D. P.; Kino, G. S.; Moerner, W. E. Toward Nanometer-Scale Optical Photolithography: Utilizing the Near-Field of Bowtie Optical Nanoantennas. *Nano Lett.* **2006**, *6*, 355–360.
50. Day, J. K.; Neumann, O.; Grady, N. K.; Halas, N. J. Nanostructure-Mediated Launching and Detection of 2D Surface Plasmons. *ACS Nano* **2010**, *4*, 7566–7572.
51. Ozbay, E. Plasmonics: Merging Photonics and Electronics at Nanoscale Dimensions. *Science* **2006**, *311*, 189–193.
52. Atwater, H. A. The Promise of Plasmonics. *Sci. Am.* **2007**, *296*, 56–63.
53. Mallin, M. P.; Murphy, C. J. Solution-Phase Synthesis of Sub-10 nm Au−Ag Alloy Nanoparticles. *Nano Lett.* **2002**, *2*, 1235–1237.
54. Leopold, N.; Lendl, B. A New Method for Fast Preparation of Highly Surface-Enhanced Raman Scattering (SERS) Active Silver Colloids at Room Temperature by Reduction of Silver Nitrate with Hydroxylamine Hydrochloride. *J. Phys. Chem. B* **2003**, *107*, 5723–5727.
55. Kneipp, K.; Wang, Y.; Kneipp, H.; Perelman, L. T.; Itzkan, I.; Dasari, R. R.; Feld, M. S. Single Molecule Detection Using Surface-Enhanced Raman Scattering (SERS). *Phys. Rev. Lett.* **1997**, *78*, 1667–1670.
56. Cai, W. B.; Ren, B.; Li, X. Q.; She, C. X.; Liu, F. M.; Cai, X. W.; Tian, Z. Q. Investigation of Surface-Enhanced Raman Scattering from Platinum Electrodes using a Confocal Raman Microscope: Dependence of Surface Roughening Pretreatment. *Surf. Sci.* **1998**, *406*, 9–22.
57. Le Ru, E. C.; Blackie, E.; Meyer, M.; Etchegoin, P. G. Surface Enhanced Raman Scattering Enhancement Factors: A Comprehensive Study. *J. Phys. Chem. C* **2007**, *111*, 13794–13803.
58. Yan, B.; Thubagere, A.; Premasiri, W. R.; Ziegler, L. D.; Dal Negro, L.; Reinhard, B. M. Engineered SERS Substrates with Multiscale Signal Enhancement: Nanoparticle Cluster Arrays. *ACS Nano* **2009**, *3*, 1190–1202.
59. Wang, H.; Halas, N. J. Mesoscopic Au "Meatball" Particles. *Adv. Mater.* **2008**, *20*, 820–825.
60. Xie, J.; Zhang, Q.; Lee, J. Y.; Wang, D. I. C. The Synthesis of SERS-Active Gold Nanoflower Tags for In Vivo Applications. *ACS Nano* **2008**, *2*, 2473–2480.
61. Liang, H.; Li, Z.; Wang, W.; Wu, Y.; Xu, H. Highly Surface-Roughened "Flower-like" Silver Nanoparticles for Extremely Sensitive Substrates of Surface-Enhanced Raman Scattering. *Adv. Mater.* **2009**, *21*, 4614–4618.
62. Yang, L.; Yan, B.; Premasiri, W. R.; Ziegler, L. D.; Negro, L. D.; Reinhard, B. M. Engineering Nanoparticle Cluster Arrays for Bacterial Biosensing: The Role of the Building Block in Multiscale SERS Substrates. *Adv. Funct. Mater.* **2010**, *20*, 2619–2628.